applied optics

Optical cavity reaching 10^{-16} frequency stability with compact optical circulator based in-coupling optics

Timm Wegehaupt,[1,2,*] Jose Sanjuan,[1,5] Martin Gohlke,[3] Pascal Grafe,[2,6] Lee Kumanchik,[1] Markus Oswald,[1,2] Thilo Schuldt,[1] and Claus Braxmaier[1,4]

[1]German Aerospace Center (DLR), Institute of Quantum Technologies, Ulm, Germany
[2]Center of Applied Space Technology and Microgravity (ZARM), University of Bremen, Bremen, Germany
[3]German Aerospace Center (DLR), Institute of Space Systems, Bremen, Germany
[4]University of Ulm, Institute of Microelectronics, Ulm, Germany
[5]Current address: Aerospace Engineering, Texas A&M University, College Station, Texas 77843, USA
[6]Current address: Max-Planck-Institut für Gravitationsphysik (Albert-Einstein-Institut) and Institut für Gravitationsphysik, Leibniz Universität Hannover, Callinstraße 38, D-30167 Hannover, Germany
*timm.wegehaupt@dlr.de

Received 23 February 2024; revised 3 April 2024; accepted 3 April 2024; posted 3 April 2024; published 22 April 2024

Future space missions will benefit from highly stable and compact optical frequency references. While many promising technologies are currently under investigation, optical cavities are a well-suited technique for applications in which relative references are required. To improve the frequency stability of optical cavities, a key step in combining high performance with compactness and robustness is the further development of in-coupling optics. Here, we present our work of using a fiber-coupled circulator based in-coupling for a high-finesse optical cavity. Implementing the new, to the best of our knowledge, in-coupling board to an extensively characterized crossed cavity set-up allows us to identify possible differences to the commonly used free-beam technique. With a frequency stability of 5.5×10^{-16} $\mathrm{Hz}^{-1/2}$ at 1 Hz and with only a slight degradation in frequency stability below the mHz range, no circulator-caused instabilities were observed.

https://doi.org/10.1364/AO.522293

1. INTRODUCTION

Optical frequency stabilization has undergone an enormous development during the recent years and has become an indispensable part in the field of metrology. Absolute frequency references like optical lattice clocks or ion clocks have overcome the best microwave references of the last decades and are currently the world's most stable clocks with frequency stability levels at 10^{-18} for integration times above 1000 s [1–3]. Optical clocks can be a new capability to address many fundamental physics questions and will probably become the new reference for a redefinition of the SI second [4,5]. Entire networks of such clocks will be able to measure the gravitational red-shift to the cm level or be a tool to search for dark matter [6–8]. More compact optical technologies like iodine-spectroscopy units are candidates to improve further the performance of future navigation satellite systems [9–11]. The great scientific advance that optical references can bring to space applications has been demonstrated by the Gravity Recovery and Climate Experiment Follow-On (GRACE-FO). There, the laser ranging interferometer (LRI) on-board the spacecraft uses a laser stabilized to an optical cavity and delivers ranging precision at the nano-meter level between the two spacecraft separated by 200 km [12,13]. Nevertheless, there is room for further improvements in measurement accuracy by increasing frequency stability.

Optical cavities are relative frequency references and are widely used in many terrestrial applications like laser pre-stabilization in optical lattice clocks or laser interferometry. In complex laboratory set-ups, optical cavities exhibit stability levels close to 10^{-17} for $1\ \mathrm{s} < \tau < 10\ \mathrm{s}$, while compact set-ups with frequency stabilities below 10^{-15} are already commercially available. However, further development is needed to unlock their full potential for space applications. A necessary decisive step for combining high performance with compactness and robustness is further development of in-coupling optics. Recently, a prototype of a monolithic cavity-based frequency reference already showed that fiber devices in combination with a minimum amount of free-beam in-coupling optics can take an important step in this direction [14].

Here, we present our work where we use a fiber-coupled optical circulator in combination with free-space alignment optics instead of a typically used fully free-space in-coupling board with a polarizing beam splitter for error signal detection. This serves as a demonstrator for future space-compatible set-ups where the free-beam components can be significantly reduced by this approach. For this set-up, no performance degradation due to the fiber circulator has been observed, and the frequency stability is one order of magnitude better than currently known fiber circulator based cavity set-ups [14].

This work is organized as follows: Section 2 contains a theoretical analysis of how an optical circulator affects the frequency stability of a cavity-stabilized laser. Sections 3 and 4 follow up with the experimental set-up to demonstrate the performance of the fiber in-coupling optics and compare it to free-beam systems. In Section 5, the results are analyzed and discussed. Section 6 closes this work with a summary.

2. OPTICAL CIRCULATORS' NOISE ANALYSES

Optical circulators are three-port non-reciprocal devices guiding light from one incoming port to the next. This allows bi-directional guiding through a single-mode fiber, ideally usable for the detection of the reflected light from an optical cavity. Compared to common set-ups using free-beam in-coupling techniques, the method presented here has several advantages. For compact highly stable optical cavities, crystalline mirror coatings offer lower thermal noise compared to standard ion beam sputtering coatings, even though current studies also see additional and partially unexplained noise sources [15,16]. However, crystalline coatings require linear polarized light to perform properly. Without the use of non-reciprocal elements, the only possibility is a beam-splitter in front of the optical cavity, which results in a light loss of at least 75%. By using an optical circulator, the light loss due to insertion loss can be reduced to <60%, and free-beam components except for the fiber injector can be completely eliminated, which increases the compactness and robustness of the system while reducing the susceptibility to external influences and misalignments.

A disadvantage of optical circulators is the so-called leakage field. The majority of the light that is coupled in port 1 is transmitted to port 2 and, similarly, light entering port 2 is mostly transmitted to port 3. Typical insertion losses are around 2 dB and are described by $F_t(\omega)$. However, a small amount of light, the leakage field, guides light from port 1 to port 3 directly with an attenuation >50 dB. We use $F_l(\omega)$ to describe such leakage. A schematic of the circulator (and the transmission and leakage field) is shown in Fig. 1. In the following, we describe the mechanism by which the leakage field affects the frequency stability of a laser locked to a high-finesse optical cavity using the Pound–Drever–Hall (PDH) technique [17,18].

For the PDH technique, the electric field must be phase-modulated so that two sidebands are generated at frequencies of $\pm\Omega$. For small modulation depths β this is described by

$$E = E_0\left[J_0(\beta)\exp^{i\omega t} + J_1(\beta)\exp^{i(\omega+\Omega)t} - J_1(\beta)\exp^{i(\omega-\Omega)t}\right], \tag{1}$$

where J_n is the Bessel function first-kind and E_0 is the amplitude of the electric field. It is important to note here that this

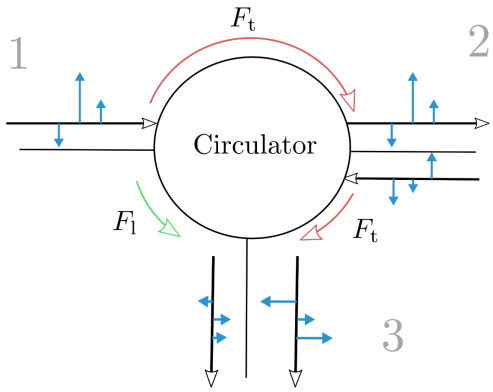

Fig. 1. Schematic of the functional principle of an optical circulator. Phase-modulated light is coupled into port 1 and transmitted to port 2 and from port 2 to 3, respectively. Simultaneously, a small amount of light from port 1 is directly transmitted to port 3.

describes a purely ideal phase modulation. In most experiments, the phase modulation is done by an electro-optical modulator (EOM). For an EOM, the phase modulation is affected by the polarization of the electrical field relative to the axis of the crystal. A description of this non-ideal phase modulation is described by [19] as

$$E_{\mathrm{EOM}} = E_0\exp^{i\omega t}\left[a\exp^{i(\beta_o\sin\Omega t+\Phi_o)} + b\exp^{i(\beta_e\sin\Omega t+\Phi_e)}\right] \tag{2}$$

and introduces a and b as alignment factors for the matching between the crystal axis of the EOM and front and rear polarizers. With $\delta_{o,e}$ and $\phi_{o,e}$ the modulation index and phase shift of the light are described, where o and e stand for ordinary and extraordinary field components. In free-beam set-ups, the phase-modulated beam then passes through a polarizing beam-splitter and a $\lambda/4$ waveplate before it reaches the front mirror of the optical cavity where it undergoes a frequency-dependent reflection or transmission described by the reflection coefficient $F(\omega)$. The back reflected light reaches a photodetector where the power of the light field is converted to voltage and is subsequently demodulated at the modulation frequency. For high modulation frequency, $\Omega \gg \delta\nu$, the dispersion term is used as error signal V_{PDH}, while [19] introduces G_{oe} as the joint gain of the photo-detection and demodulation process:

$$V_{\mathrm{PDH}} = E_0^2 G_{\mathrm{oe}} A\Im\left[F(\omega)F^*(\omega+\Omega) - F^*(\omega)F(\omega-\Omega)\right]. \tag{3}$$

In the ideal case for a cavity on resonance with high modulation frequency, ideal meaning an impedance-matched cavity with perfect alignment and mode matching, the sidebands are totally reflected, $F(\omega\pm\Omega)\approx -1$, and the carrier is transmitted, $|F(\omega)| = 0$. However, as it is experimentally impossible to achieve this condition and thus a contrast of 100%, $|F(\omega)| \neq 0$, and the demodulated signal also depends on the so-called residual amplitude modulation (RAM). This is generated by the birefringence of the EOM and parasitic etalons between optical free-beam components for classical set-ups. RAM is created by the unequal amplitude of the modulation sidebands and results in an offset of the demodulated error signal [20].

For the use of an optical circulator for the frequency stabilization to an optical cavity, it can thus be assumed that the circulator's leakage field behaves like a parasitic etalon between

the $\lambda/4$ wave-plate and the optical cavity in typical free-beam set-ups. A detailed analysis of this phenomenon is shown in [19] and can therefore be adapted to the following. The reflection coefficient $F(\omega)$ is for the circulator case replaced by a sum of the refraction coefficient of the surpassed medium,

$$F(\omega) = F_{\mathrm{l}}(\omega) + F_{\mathrm{t}}(\omega)^2 F_{\mathrm{r}}(\omega), \tag{4}$$

while $F_{\mathrm{l}}(\omega)$ describes the leakage field from port 1 to 3, and $F_{\mathrm{t}}(\omega)$ the transmission from port 1 to port 2 and port 2 to port 3, respectively. No difference is assumed here for the two passes, due to the symmetrical structure of circulators. $F_{\mathrm{r}}(\omega)$ is now the reflection coefficient of the optical cavity for the nonideal case. Inserting Eq. (4) into Eq. (3) can then analogous to [19] be simplified to

$$V_{\mathrm{RAM}} = V_{\mathrm{RAM_t}} + V_{\mathrm{RAM_l}} + V_{\mathrm{RAM_{t,l}}}, \tag{5}$$

with $V_{\mathrm{RAM_t}}$ describing the RAM caused by the circulator transmission, $V_{\mathrm{RAM_l}}$ as a component caused by the leakage field only, and $V_{\mathrm{RAM_{t,l}}}$ as the RAM due to the interaction of the leakage field and the back reflected light of the optical cavity. Similarly to free-beam in-coupling layouts, the magnitude of the RAM is a function of frequency due to the frequency dependence of the reflection coefficients. The resulting frequency instability is then dependent on their change over time. Therefore, the reflectivity and length are important for the impact a parasitic etalon has on the RAM. In general, longer etalons create shorter free spectral ranges (FSR) and need to be avoided, as they will create large power differences in the sidebands. Needless to say, the reflectivity of the surfaces creating a parasitic etalon should be as small as possible. Common approaches are anti-reflective (AR) coatings on optical components, a reasonable distance choice between the components, and slightly tilted optical components [21].

For the circulator configuration, the frequency dependency of the transmission and leakage field needs to be further investigated. To do so, a power stabilized (7 mW) 1064 nm non-planar ring oscillator (NPRO) laser with linear polarization is coupled to the slow axis of port 1 of a polarization maintaining optical circulator with 1 m optical fiber length and FC-APC connectors, where a high sensitive Newport 2936-R power-meter is in a first experiment connected to port 3. The minimum measurable power is 20 pW. At the same time, a frequency scan of 1 GHz is applied to the slow modulation port of the laser. The result of one scan is shown in Fig. 2. With -58 dB up to -66 dB, it is well below the minimum value for the directivity of -50 dB from the manufacturer specifications, which, in turn, does not include connectors. At the same time, there is a clear frequency dependence that Is largely independent of whether the laser frequency is increasing (blue line) or decreasing (red line). However, for long measurements over multiple scans, a change over time can be observed. In a second experiment, the transmission from port 1 to port 2 is analyzed, and no clear frequency dependency is observed. Derived from the measurements, it can be inferred that the circulator acts for the leakage field like a parasitic etalon with an FSR between 100 MHz and 150 MHz. This corresponds to a length between 1 m and 1.5 m. As 1 m is the used optical fiber length of each port, it is considered that the FSR could be further increased by shortening the fibers and splicing optical and electro-optical components closer together.

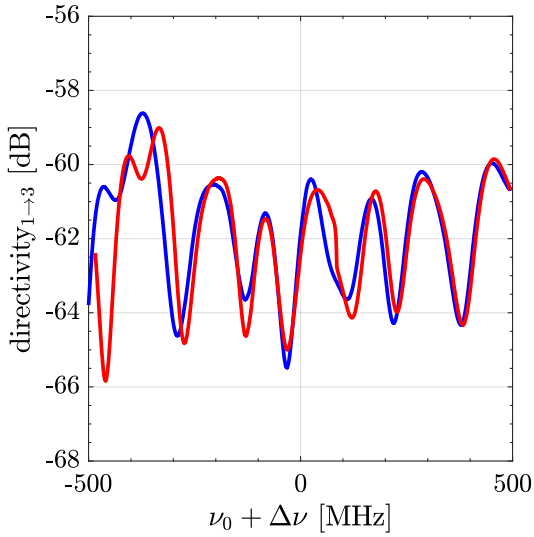

Fig. 2. Measured directivity between port one and port three for a frequency modulated laser at about 1064 nm. The blue line indicates the rising edge of the frequency scan, while the red line corresponds to the falling side.

Even though the FSR of this parasitic etalon is smaller than in typical free-beam layouts, the impact of such leakage field caused RAM is due to the directivity of about -60 dB expected to be rather low while a proper theoretical model that allows for a noise prediction requires further analysis. In any case, the RAM caused by crystal birefringence and the circulator results in a frequency offset,

$$\Delta\nu_{\mathrm{offset}} = \frac{V_{\mathrm{RAM}}}{D}, \tag{6}$$

where D is the discriminator slope, i.e., the error signal slope of PDH, and is proportional to the finesse of the optical cavity, resulting in an inversely proportional dependency between finesse and RAM-caused frequency instability. This also makes high-finesse cavities less sensitive to RAM-induced instabilities of optical circulators.

This leads to the conclusion that the advancing technological development of optical fiber components and coatings of mirrors make the use of circulators in frequency stabilization possible and provides a great improvement for future compact and mechanically stable set-ups.

3. SET-UP DESCRIPTION

To demonstrate the functionality of a circulator based in-coupling technique, an 8.7 cm long crossed cavity is used as reference. It has a cube design patented by the National Physical Laboratory (NPL) with a spacer made out of ultra-low expansion glass (ULE) and fused silica (FS) mirrors optically contacted to it [22]. ULE compensation rings on the backside of the mirrors shift the zero crossing point of the whole system to room temperature. Both pairs of mirrors consist of a combination of one flat and one curved ($R = 1$ m) mirror. The cavity is mounted in a tetrahedral configuration in an aluminum frame to minimize the vibration sensitivity to an order of 1×10^{-10} g^{-1} as demonstrated in [22]. A picture of

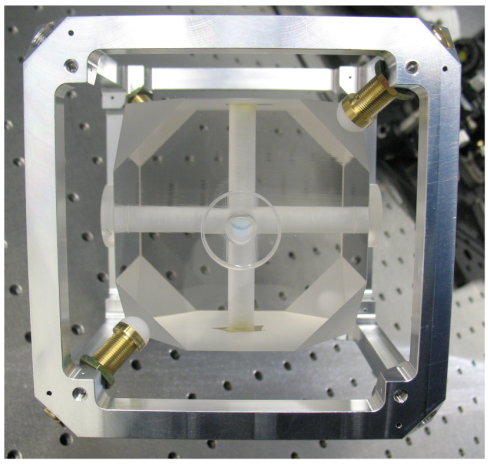

Fig. 3. Crossed-cavity with 8.7 cm optical path length mounted in a tetrahedral configuration.

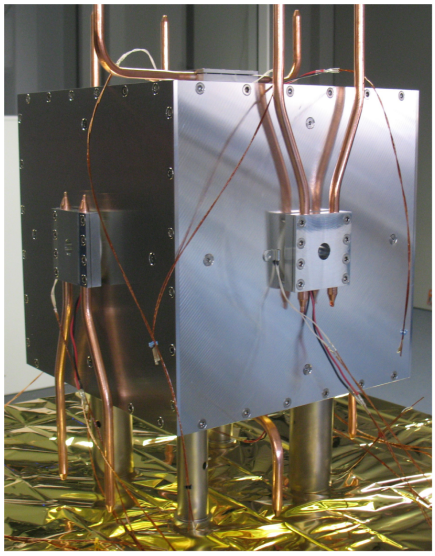

Fig. 4. Optical cavity covered by five thermal shields with Peltier elements attached. The shown copper heat pipes will be connected to the vacuum chamber, which acts as heat sink, after integration.

the set-up is shown in Fig. 3. The aluminum frame is covered by five thermal shields, the outermost one is actively stabilized by Peltier elements. Attached to the Peltier elements, copper heat pipes provide a thermal connection to the vacuum chamber, which is used as a heat sink as shown in Fig. 4. The whole cubic set-up is placed in a vacuum chamber operating at 10^{-7} mbar. One optical path is used with a classical set-up consisting of a large free-beam in-coupling breadboard rigidly mounted to the vacuum chamber and an extra laser-board, placed on the same optical table. This whole set-up has been fully characterized against a second duplicated system and is explained in more detail in [23]. Here, the set-up is called *free-beam set-up*.

The second optical path of the crossed cavity was unused before and provides the basis for the new compact demonstrator, which is called *circulator set-up* here. A schematic is shown in Fig. 5. The circulator set-up consists of three parts: a laser breadboard, an in-coupling breadboard, and the electronics. The laser

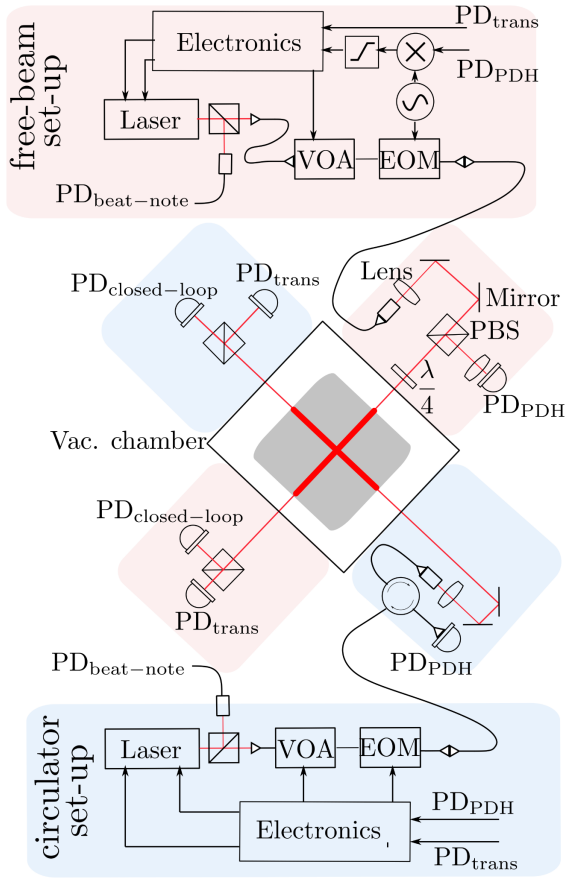

Fig. 5. Schematic of the experimental set-up, focused on the optical part with the corresponding PDH-frequency stabilization scheme. Its center shows the crossed cavity with two optical paths. One is used for a traditional free-beam in-coupling technique, highlighted in red. For the second optical path, an optical circulator is mounted on a small breadboard in front of the vacuum chamber to reduce the free-beam components and make the set-up more robust and compact, highlighted in blue.

breadboard includes a Nd:YAG NPRO Laser at 1064 nm that is coupled into a polarization maintaining (PM) optical fiber and passes a MEMS-based electrical variable optical attenuator and an EOM driven at 5 MHz to generate the sidebands for the PDH-technique. To improve the in-coupling optics by reducing the optical free-beam components and make the set-up more robust, a fiber-coupled polarization-maintaining optical circulator is mounted on a small in-coupling breadboard in front of the vacuum chamber. Modulated light from the fiber-coupled EOM passes an in-fiber polarizer and is coupled into port 1 of the circulator. Port 2 is collimated and mode matched by a 750 mm lens towards the cavity before passing an optical window to enter the vacuum chamber. All components have anti-reflective coatings to avoid additional parasitic etalons. The beam-to-cavity mode alignment is done with two adjustable optical mirrors and can be replaced in future experiments by a customized designed fiber collimator directly bonded to the thermal shield of the optical cavity [24]. Back-reflected light from the flat cavity mirror is refocused along the same optical path back into the PM fiber, connected to the collimator. This requires an optimal mode matching, where the Gaussian beam

waist is located directly on the flat mirror of the cavity. This is achieved by previous calculations and subsequent beam-propagation measurements. Based on the principle of an optical circulator, light is forwarded from port 2 to 3. Port 3 is connected to a fiber-coupled photodiode (Thorlabs PDA10CS EC) detecting the modulated PDH error signal.

4. DIGITAL LOCK-IN ELECTRONICS

The data processing is performed by a compact digital electronic set-up made up of a CompactRIO Single-Board Controller (National Instruments) and an AD/DA data conversion card (Terasic) combined by a self-developed adapter card using the sbRIO RIO Mezzanine Card (RMC)-Connector—cf. Fig. 6. All three devices together result in a 80 MHz fast running FPGA with two 80 MHz analog inputs and outputs, plus several slow ones. The signal reflected from the cavity is converted into a 14-bit signal and is internally demodulated in quadrature with the EOM driving signal. Two digital PID controllers are implemented to tune the laser's piezo- and Peltier-current for high- and low-bandwidth laser frequency control, respectively. Additionally, an intensity control loop is implemented to stabilize the transmitted intensity to 100 μW by using a photodiode (Thorlabs PDA36A) behind the vacuum chamber as reference. With a 50/50 beamsplitter, a second photodiode (Thorlabs PDA36A2) is installed for intensity out-of-loop test measurements.

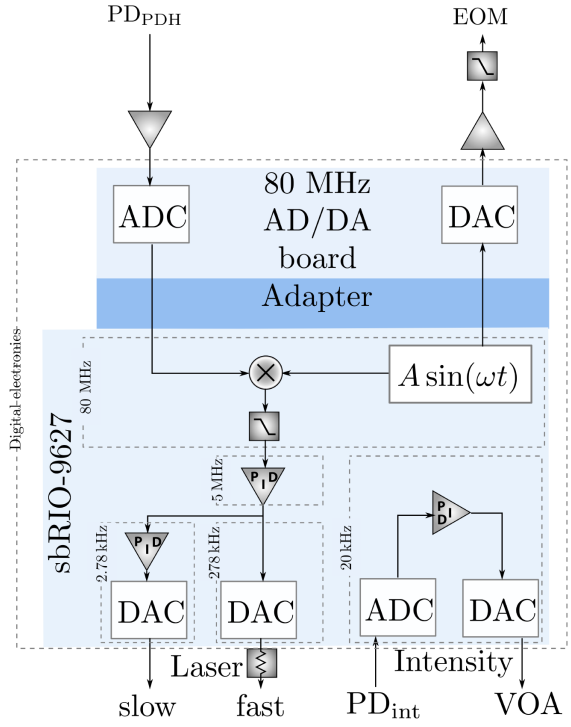

Fig. 6. Schematic showing the compact digital control electronics consisting of an sbRIO-9627 combined with a Terasic 80 MHz AD/DA card. In this first iteration, the latter is clocked with an external 80 MHz not shown in the sketch. The gray numbers indicate the different loop frequencies.

5. STABILITY RESULTS AND NOISE SOURCES

The frequency stability is determined by performing a beat measurement at ≈ 900 MHz between two lasers stabilized to the orthogonal paths in the cavity using standard in-coupling optics and the circulator set-up. Parts of both lasers are coupled into a 50/50 fiber combiner whose second end is connected to a fast photodiode (New focus 1544b). The output is measured by a frequency counter (Pendulum CNT-91) with up to 10 Hz sampling frequency.

In [23], the fractional frequency stability of the free-beam set-up, shown in Fig. 7, has been analyzed in detail, and the limiting factors are well outlined. At frequencies above 2 mHz, the performance is mainly limited by fiber noise caused by vibrations, temperature fluctuations, and acoustic noise. For frequencies between 200 μHz and 2 mHz, intensity noise has been identified as the dominating noise source. Below 200 μHz, mainly beam pointing noise together with temperature fluctuations takes over. The fractional frequency stability for a one-day measurement between the free-beam set-up and the circulator is shown in Fig. 7 in units of square root of power spectral density, also referred to as amplitude spectral density (ASD), and scaled by a factor of $1/\sqrt{2}$ to represent the stability of one set-up. In the following, this measurement is labeled *circulator set-up*.

For frequencies between 0.35 Hz and 2 mHz, the circulator set-up against the free-beam set-up measurement is almost on the same level as the previous free-beam set-up reference measurement and shows only small deviations. On long time scales, below 2 mHz, the circulator versus free-beam measurement is slightly degraded. At frequencies above 0.35 Hz there is a factor of 2 improvement. However, this improvement cannot be attributed to the circulator set-up with certainty, as the free-beam set-up is also part of the measurement.

To understand these results, the measuring method has to be discussed in detail and noise sources further analyzed. As explained before, these measurements were performed by using

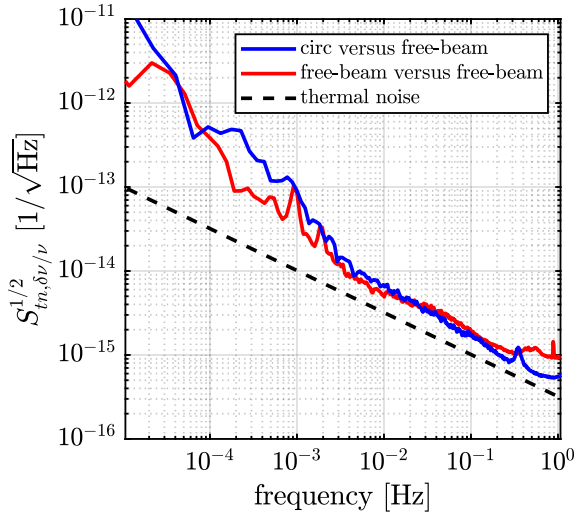

Fig. 7. Fractional frequency stability in the square root of power spectral density for a crossed cavity set-up with an optical circulator based in-coupling set-up. For comparison, a measurement of two identical set-ups with traditional free-beam in-coupling optics from [23] is shown in red. The black dashed line represents the thermal noise limit of the cavity.

a crossed cavity, while the in-coupling optics, electro-optical components, and electronics are different. Compared with two individual systems, a crossed cavity offers a rejection of common mode noise sources. Common mode noise sources are defined as noise levels that are canceling each other out in the measured beat note due to similar effects on the laser frequency. In our case, these are only noise levels originating from the cavity itself. However, it is expected that all dominating noise sources apart from frequency noise caused by temperature fluctuations are not common noise. Temperature noise scales for two independent systems with the laser frequency ν_L, coefficient of thermal expansion α, and temperature changes δT [25]:

$$\delta\nu = \alpha\nu_L\delta T. \tag{7}$$

For a crossed cavity set-up, assuming a uniform temperature distribution and both coefficients of thermal expansion (CTE) are exactly the same, it only scales with the beat-note frequency, though the frequency noise could be around five orders of magnitude smaller compared to two independent systems. However, this does not correspond to a real experiment, as the CTE depends on the length of the spacer as well as the mirrors and the size of the compensation rings. With a measurement of two lasers on one optical path of the cavity, we determined the FSR and therefore the cavity length, which is different by 10 µm. As the temperature control is set for the zero crossing point of the free-beam in-coupling arm, it is likely that the 10 µm longer cavity arm used for the circulator is working at a CTE with up to two orders of magnitude larger. In addition, variances in the temperature distribution increase frequency instabilities due to thermal variations, though a long-term performance comparable to two independent systems is expected.

As an additional noise source at low frequencies, it is expected that frequency noise due to pointing noise is accounting for deviations. For the free-beam in-coupling, the breadboard is rigidly mounted to the vacuum chamber, while for the circulator in-coupling breadboard no connection to the chamber exists. Here, a standard aluminum breadboard has been placed on 1-inch posts on an optical table in front of the chamber, which can lead to larger pointing noise at long timescales compared to the rigidly mounted breadboard.

Between 2 mHz and 200 µHz the frequency stability may also be affected by long-term intensity instabilities. This has been proven already for the free-beam in-coupling set-ups for the peaks at 1 mHz and 2 mHz, while using InGaAS-based photodiodes. For the circulator set-up, Si-based photodiodes have been installed instead, as they happened to be on hand in our lab. The latter are more sensitive to temperature fluctuations compared to InGaAs diodes, which lead to larger frequency fluctuations.

After the free-beam versus free-beam measurement and before the circulator versus free-beam measurement, the fiber routing of the two set-ups involved in the second measurement was updated, which may explain small deviations above 2 mHz. The improvement above 0.35 Hz by a factor of two cannot necessarily be attributed to the updated fiber routing and must be investigated further.

In any case, the circulator does not add any extra noise to the system compared to a free-beam versus free-beam set-up, which paves the way for future compact and mechanically stable set-ups. For completeness, the frequency stability is shown in Fig. 8 in the Allan deviation metric, which shows a frequency stability of $\sigma < 8 \times 10^{-16}$ for $1 < \tau < 10$ s and $\sigma < 6 \times 10^{-15}$ for $10 < \tau < 1000$s.

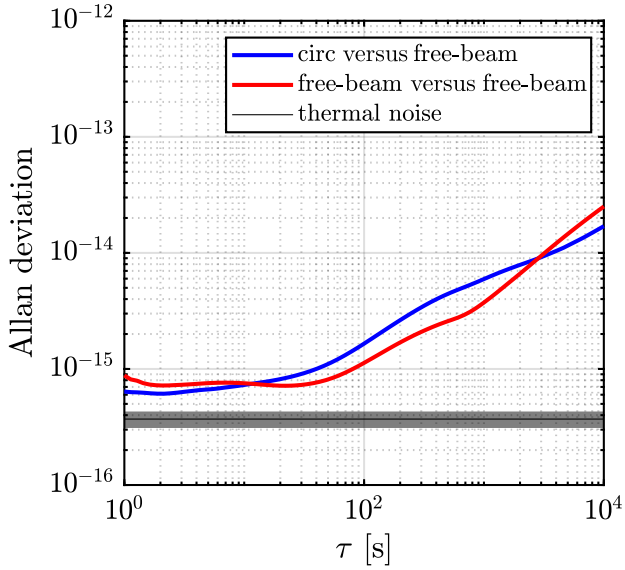

Fig. 8. Allan deviation for a crossed cavity set-up with an optical circulator based in-coupling set-up in blue and a measurement of two identical set-ups with traditional free-beam in-coupling optics from [23] shown in red. Both measurements are linear detrended. The black dashed line represents the thermal noise limit of the cavity.

6. SUMMARY

The work presented here has demonstrated the suitability of an optical circulator for high-performance optical cavity stabilization. With a demonstrated frequency stability of 5.5×10^{-16} $\mathrm{Hz}^{-1/2}$ at 1 Hz, almost similar to a free-beam in-coupled system, and with only a slight degradation in frequency stability below the mHz range, no parasitic etalon instabilities were observed. The differences are primarily attributed to intensity noise and long-term pointing noise. With the principle demonstrated here, it is possible to reduce free-beam components in future set-ups when using a fiber circulator. This would be a further improvement towards more robust and compact set-ups also with respect to emphasis on space compatibility as the here-demonstrated frequency stability is fulfilling the requirements of next generations of gravity missions. A new compact demonstrator based on an optical circulator is already under development. This will also use the here-introduced digital, compact, and cost-effective electronics.

Funding. Deutsches Zentrum für Luft- und Raumfahrt; Helmholtz Association (ZT-007).

Acknowledgment. This work is supported by the Helmholtz-Gemeinschaft Deutscher Forschungszentren e.V. (ADVANTAGE, Advanced Technologies for Navigation and Geodesy) and by the German Aerospace Center (DLR e.V.), with funds provided by the Federal Ministry of Economic Affairs and Climate Action, within the project COMPASSO. Within the cavity development, fruitful cooperation with NPL is acknowledged.

Disclosures. The authors declare no conflicts of interest.

Data availability. Data underlying the results presented in this paper are not publicly available at this time but may be obtained from the authors upon reasonable request.

REFERENCES

1. S. M. Brewer, J.-S. Chen, A. M. Hankin, *et al.*, "$^{27}Al^{+}$ quantum-logic clock with a systematic uncertainty below 10^{-18}," Phys. Rev. Lett. **123**, 033201 (2019).
2. T. Nicholson, S. Campbell, R. Hutson, *et al.*, "Systematic evaluation of an atomic clock at 2×10^{-18} total uncertainty," Nat. Commun. **6**, 6896 (2015).
3. N. Huntemann, C. Sanner, B. Lipphardt, *et al.*, "Single-ion atomic clock with 3×10^{-18} systematic uncertainty," Phys. Rev. Lett. **116**, 063001 (2016).
4. P. Gill, "Is the time right for a redefinition of the second by optical atomic clocks?" J. Phys. Conf. Ser. **723**, 012053 (2016).
5. N. Dimarcq, M. Gertsvolf, G. Mileti, *et al.*, "Roadmap towards the redefinition of the second," arXiv, arXiv:2307.14141 (2023).
6. W. McGrew, X. Zhang, R. Fasano, *et al.*, "Atomic clock performance enabling geodesy below the centimetre level," Nature **564**, 87–90 (2018).
7. P. Wcisło, P. Morzyński, M. Bober, *et al.*, "Experimental constraint on dark matter detection with optical atomic clocks," Nat. Astron. **1**, 0009 (2016).
8. A. Derevianko and M. Pospelov, "Hunting for topological dark matter with atomic clocks," Nat. Phys. **10**, 933–936 (2014).
9. T. Schuldt, M. Gohlke, M. Oswald, *et al.*, "Optical clock technologies for global navigation satellite systems," GPS Solut. **25**, 83 (2021).
10. K. Döringshoff, T. Schuldt, E. Kovalchuk, *et al.*, "A flight-like absolute optical frequency reference based on iodine for laser systems at 1064 nm," Appl. Phys. B **123**, 183 (2017).
11. G. Giorgi, T. D. Schmidt, C. Trainotti, *et al.*, "Advanced technologies for satellite navigation and geodesy," Adv. Space Res. **64**, 1256–1273 (2019).
12. K. Abich, A. Abramovici, B. Amparan, *et al.*, "In-orbit performance of the grace follow-on laser ranging interferometer," Phys. Rev. Lett. **123**, 031101 (2019).
13. B. Sheard, G. Heinzel, K. Danzmann, *et al.*, "Intersatellite laser ranging instrument for the grace follow-on mission," J. Géod. **86**, 1083–1095 (2012).
14. Y. Luo, H. Li, Y.-Q. Li, *et al.*, "Prototype of a monolithic cavity-based ultrastable optical reference for space applications," Appl. Opt. **60**, 2877–2885 (2021).
15. G. D. Cole, W. Zhang, M. J. Martin, *et al.*, "Tenfold reduction of Brownian noise in high-reflectivity optical coatings," Nat. Photonics **7**, 644–650 (2013).
16. J. Yu, S. Häfner, T. Legero, *et al.*, "Excess noise and photoinduced effects in highly reflective crystalline mirror coatings," Phys. Rev. X **13**, 041002 (2023).
17. R. W. Drever, J. L. Hall, F. V. Kowalski, *et al.*, "Laser phase and frequency stabilization using an optical resonator," Appl. Phys. B **31**, 97–105 (1983).
18. E. D. Black, "An introduction to Pound–Drever–Hall laser frequency stabilization," Am. J. Phys. **69**, 79–87 (2001).
19. H. Shen, L. Li, J. Bi, *et al.*, "Systematic and quantitative analysis of residual amplitude modulation in Pound–Drever–Hall frequency stabilization," Phys. Rev. A **92**, 063809 (2015).
20. E. A. Whittaker, M. Gehrtz, and G. C. Bjorklund, "Residual amplitude modulation in laser electro-optic phase modulation," J. Opt. Soc. Am. B **2**, 1320–1326 (1985).
21. P. Ehlers, I. Silander, J. Wang, *et al.*, "Fiber-laser-based noise-immune cavity-enhanced optical heterodyne molecular spectrometry incorporating an optical circulator," Opt. Lett. **39**, 279–282 (2014).
22. S. Webster and P. Gill, "Force-insensitive optical cavity," Opt. Lett. **36**, 3572–3574 (2011).
23. J. Sanjuan, K. Abich, M. Gohlke, *et al.*, "Long-term stable optical cavity for special relativity tests in space," Opt. Express **27**, 36206–36220 (2019).
24. T. Wegehaupt, J. Sanjuan, M. Gohlke, *et al.*, "Optical cavity setup for future hybrid lock concept," in *Joint Conference of the European Frequency and Time Forum and IEEE International Frequency Control Symposium (EFTF/IFCS)* (2022), pp. 1–4.
25. J. Sanjuan, N. Gürlebeck, and C. Braxmaier, "Mathematical model of thermal shields for long-term stability optical resonators," Opt. Express **23**, 17892–17908 (2015).